Journal Pre-proof



Modelling of thermal conductivity and nonlinear mechanical behavior of straw insulation composite by a numerical homogenization approach

Brahim Ismail, Naima Belayachi, Dashnor Hoxha, Laurent Arbaret

PII: S2352-7102(21)01002-0

DOI: https://doi.org/10.1016/j.jobe.2021.103144

Reference: JOBE 103144

To appear in: *Journal of Building Engineering*

Received Date: 30 March 2021

Revised Date: 29 July 2021

Accepted Date: 14 August 2021

Please cite this article as: B. Ismail, N. Belayachi, D. Hoxha, L. Arbaret, Modelling of thermal conductivity and nonlinear mechanical behavior of straw insulation composite by a numerical homogenization approach, *Journal of Building Engineering* (2021), doi: https://doi.org/10.1016/j.jobe.2021.103144.

This is a PDF file of an article that has undergone enhancements after acceptance, such as the addition of a cover page and metadata, and formatting for readability, but it is not yet the definitive version of record. This version will undergo additional copyediting, typesetting and review before it is published in its final form, but we are providing this version to give early visibility of the article. Please note that, during the production process, errors may be discovered which could affect the content, and all legal disclaimers that apply to the journal pertain.

© 2021 Published by Elsevier Ltd.

Journal Pre-proof

Modelling of thermal conductivity and nonlinear mechanical behavior of straw insulation composite by a numerical homogenization approach

Brahim ISMAIL[1], Naima BELAYACHI[1], Dashnor HOXHA[1], Laurent ARBARET[2]

[1] Université d'Orléans, INSA Centre Val de Loire, Université de Tours, Laboratoire de Mécanique Gabriel Lamé Polytech Orléans, 8 rue Léonard de Vinci, 45072 Orléans, France

[2] ISTO, UMR 7327, Université d'Orléans, CNRS, BRGM, 1A rue de la Férollerie, 45071, Orléans, France

Corresponding author :

Naima Belayachi

Tel : 330238492502

Fax : 330238417063

E-mail address : naima.belayachi@univ-orleans.fr

Postal address : Laboratoire LaMé, Polytech'Orléans

8 Rue Léonard De Vinci

45072, Orléans cedex 2, France

Highlights

- Thermal conductivity and mechanical behavior of new straw composite were modeled using 3D numerical homogenization.
- X-ray micro-tomography was used to determine volume fractions of composite constituents.
- A particular shape of inclusion "3D-curved spherocylindrical" was adopted to represent plant aggregates.
- The numerical homogenization method used, allowed to predict the mechanical strength of the new bio-based composite.

Journal Pre-proof

Abstract

Bio-based materials have been extensively studied in recent decades. These materials based on vegetable aggregates are highly heterogeneous, and their complex behaviour depends on the behaviour of the constituents as well as their spatial distribution, size, and shape. Classically, homogenization methods are used for the prediction of the behaviour of heterogeneous materials because they allow to take into-account the microscopic phenomena and characteristics governing the macroscopic behaviour at a considered scale. In the case of composite materials, the use of this prediction approach allows to optimize the properties according to some criteria while limiting often expensive and time-consuming experimental tests. This paper aims to predict the effective thermal conductivity and model the mechanical behaviour of a bio-composite based on lime and cereal straw. A numerical homogenization approach was adopted to consider the complex microstructure of these biobased materials. An experimental characterization of the composites was carried out to describe the microstructure of the material (size, orientations, and shape of aggregates). X-Ray micro tomography observation was performed to determine volume fraction of the different phases of the biocomposite.

A statistical approach was also used to determine the size of the Representative Volume Element (RVE) of the studied material for different distributions of heterogeneities. Then, numerical simulations of the thermal and mechanical behavior of composite was carried out. The results show the need to take into account an interphase between the straw aggregates and the matrix as well as the effect of the vegetal aggregates on the hydration of the binder to accurately predict the effective properties of the material.

Keywords: Straw Composite, Thermal Conductivity, Mechanical Behavior, X-Ray Micro-tomography, Representative Volume Element (RVE), Modeling, Numerical Homogenization,

1 Introduction

Bio-based materials have a growing interest in improving building thermal performance and reduces the carbon emissions of the construction sector. Generally, these materials are based on vegetable, renewable aggregates and organic/inorganic binders [1–7]. Numerous scientific studies have been carried out on the development and the experimental characterization of these composites. They showed interesting thermal, acoustic insulation capacities and excellent hydric properties of these materials [8–14] combined with interesting characteristics such as low energy consumption, low carbon footprint, low cost, low density and biodegradability [15–19]. The properties of the bio-composites depend strongly on the fraction and the morphology of the constituents, in particular the type and content of binder, the distribution and the size of the aggregates [20,21]. It has also been reported in the literature that the relative humidity significantly impacts the thermal conductivity of the composites due to their hygroscopic nature [22–24].

Several works in the literature have attempted to determine thermal and mechanical macroscopic properties of this type of materials by taking into account their microstructure [22, 24–27]. In all these works self-consistent homogenization based on a spherical inclusion (bicomposite or tricomposite) was used. However, the predictions of this method become medicor when the binder fraction decreases below 19% of the volume because of the assumption of the matrix continuity which is not verified for this case [25]. Akkaoui et al. 2017 [28] have used self-consistent method combined with a composite-sphere like microstructure to predict the Young modulus of a wood aggregate concrete. Following these authors the representation of the microstructure of wood concrete as an aggregation of solid grains surrounded by a layer of binder and porosity represented by voids among these

aggregates seems to be a better alternative of structure description as compared to hollow spherical inclusions microstructure used by [25]. The results obtained, using this microstructure representation are in good agreement with the experimental measurements and model has been considered according to the authors as a predictive tool to optimize the elastic properties of wood aggregate concrete [28]. However, the use of such microstructure representation remains limited to the case of materials with an intergranular porosity of less than 50% which is the percolation limit of the self-consistent scheme.

In a recent study, Tran-Le et al. 2018 [29] have developed a novel analytical model approach to predict effective thermal conductivity tensor of lime-hemp concrete by taking into account the anisotropy, size, orientation of aggregates and the interface between the binder and aggregates. This approach could be seen as an extension of the Eshelby's solution to several ellipsoidal inclusions. By comparing results of their model with experimental measures, they concluded on the necessity of taking into account in modeling the thermal contact resistance between the aggregates and the binder, in order to fit the observed values of thermal conductivity. This model constitutes a suitable prediction tool of the thermal conductivity of hemp concrete, but it is only valid in the dry state.

Couture et al. 2017 [30] also noted that the pre-compaction used during the manufacturing of the materials leads to anisotropy of thermal conductivity at the macroscopic scale. The authors adopted a numerical approach based on finite element calculations to model the thermal conductivity of hemp concrete. The hemp aggregates were represented by cylindrical inclusions aligned in the same direction and arranged randomly. However, their volume fraction does not exceed 15%. The authors confirmed by the simulations carried out, the transverse isotropic character of thermal conductivity of hemp concrete. Mom et al. 2011 [31] used an iterative homogenization approach based on finite element calculations to model the thermal conductivity of hemp concrete with bar shaped particles and high porosity rates. This

approach made it possible to take into account the anisotropy of the material and to represent the hemp particles by plate inclusion. The authors compared the results of this model with the experimental measurements of Cerezo 2005 [25] and Nguyen et al. 2018 [32]. They concluded that the multi-scale iterative technique adopted, provides a satisfactory prediction of thermal conductivity.

The knowledge of the effective properties of other lightweight insulation materials is also a topic of actual interest of foam concretes, due to their wide use in construction project. This special class of porous materials with cellular microstructure have been extensively studied by using periodic homogenization method. Low et al 2020 [33] studied the influence of boundary conditions on the computation of the effective thermal conductivity of foams with a high porosity of 74%. Three types of foam geometries were used, namely, unit cell-based structures, digitally generated periodic foams, and tomography-reconstructed real foams. The authors have shown the importance of choosing the appropriate boundary conditions for the geometries used to accurately estimate the effective thermal conductivity. Miled et al 2016 [34] proposed a three dimensional finite Element Method for the prediction of the effective thermal conductivity of foam concretes having a porosity ranging between 0 and 0.68. They have reported that the effective thermal conductivity of foam concretes can be predicted according to their porosity by a general power law. Their results also showed no significant effect of the pores size distribution, and spatial distribution on the effective thermal conductivity of foam concretes.

The present study aims to predict the thermal conductivity and model mechanical behavior of straw insulation composite developed in previous works by authors [2,35]. The objective is the mixtures optimization by using predictive capacity of homogenization approach in order to limit experimental tests. A numerical homogenization approach is adopted to take into account a complex microstructure more representative of the real composite, considering the

Journal Pre-proof

size, the shape, the orientation of the aggregates with high rate and also the significant intergranular porosity. In addition to Young's modulus prediction of biobased concrete, a subject very often treated in abundant research, the modeling approach proposed aims at description of full nonlinear mechanical behavior of this biocomposite. In fact, the mechanical strength in compression is an essential parameter to be determined for all constructing materials. So, the proposed non-linear modeling should be a tool to estimate the mechanical strength of straw concrete as a function of the structure and composition. Using the model makes it possible to optimize the mixtures by taking into account two criteria of use, a better thermal performance and a good mechanical strength for material's buildability.

2 Materials and characterization methods

2.1 Materials

Two composites were selected from previous work [35] for this investigation. The first is based on lime with a ratio of Water/Binder = 1.1 and Straw/Binder = 0.2 and the second prepared with the same Water/Binder ratio and a higher ratio of Straw/Binder = 0.4 with a binder consisting of lime and 20 % gelatin. The use of this biopolymer allows increasing of the ratio of vegetal aggregates. The description of raw materials and manufacturing procedure is detailed in the work of Ismail et al. 2020 [35]. The composites are denoted respectively C1 and C2, as indicated in Tab. 1.

Composites	Binder	Straw/Binder (kg/kg)	Water/Binder (kg/kg)	Density (kg/m^3)
C1	Lime	0.2	1.1	450
C2	Lime+20%gelatin	0.4	1.1	300

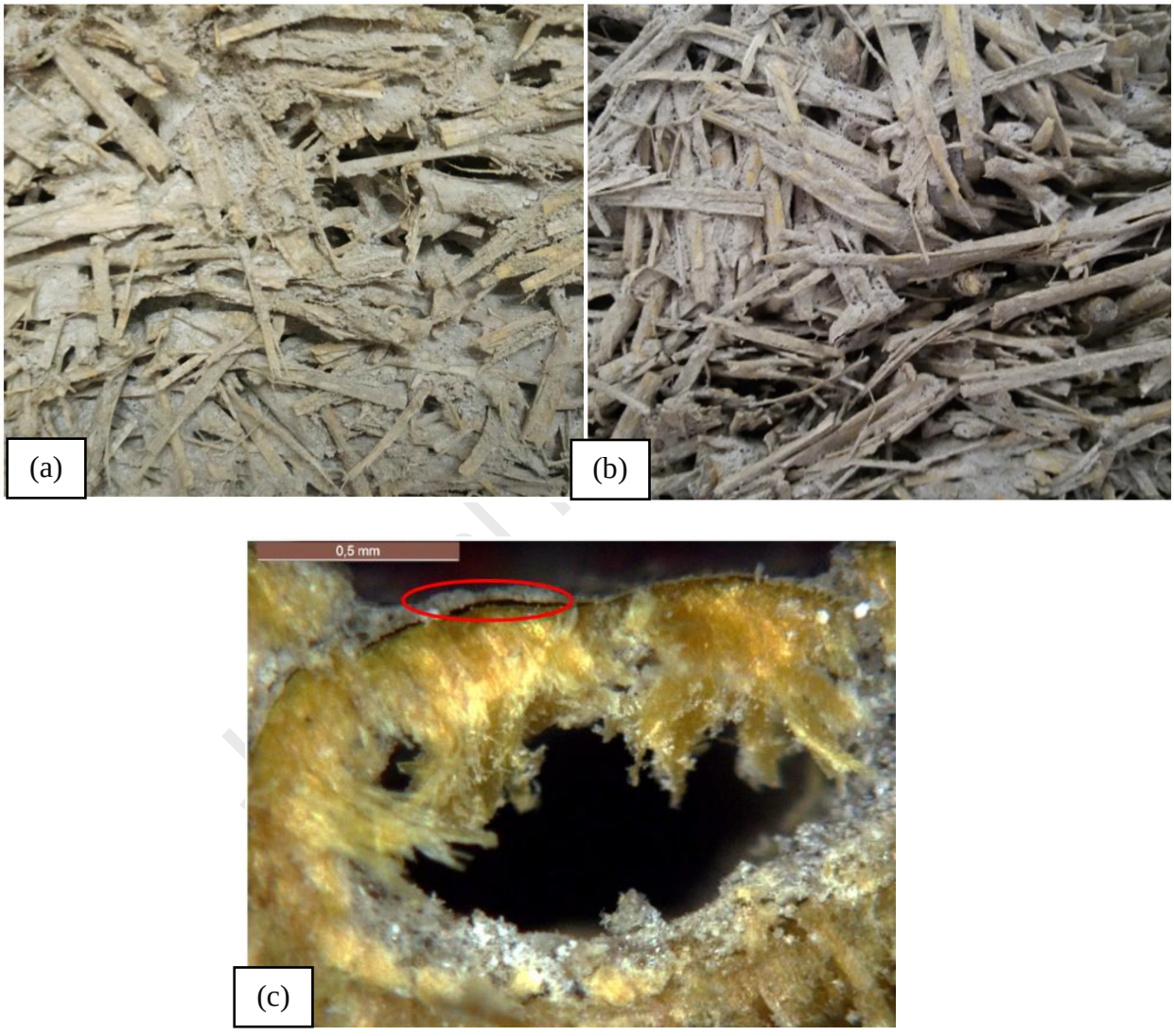
Tab. 1. Composite designation and detailed mixture proportions

Fig. 1 shows the appearance of the two composites. We can observe that in both cases, the aggregates are coated with a layer of binder and voids between them. These coated aggregates

154 are connected by binder bridges. There are randomly arranged and not always straight but are
155 curved due to their low stiffness. We can also observe in Fig 1c the presence of the interphase
156 or decohesion between the straw aggregate and the matrix.

157

158



159

160 **Fig. 1.** Appearance of composites (a) C1 (with a high binder content) (b) C2 (with a low
161 binder content) (c) microscope visualization of the straw aggregate–matrix interface

2.2 Experimental characterization

2.2.1 X-ray micro-tomography: volume fractions of the constituents:

In order to determine the fraction of each constituent phase in composites, micro computed tomography (microCT) analyses were performed at the Institut des Sciences de la Terre d'Orléans (Orléans, France) on a Nanotom 180NF from Phoenix X-Ray (Fig. 2). We used an accelerating voltage of 180 kV, a filament current of 170 nA, and an operating voltage of 120 V. During acquisition, the sample rotates 360°, allowing the instrument to take successive images, covering all angles. Microtomography analysis was performed on representative samples of 3 × 3 × 3 cm^3 which resulted in a resolution of 17 μm^3 per voxel. After the analysis, the stack of 2D images is processed to construct a volume, manually extracted using the software VG-Studio Max 1.2. A 3^3 median filter was applied to obtain homogeneous and clear images. The dataset was processed by VGStudio MAX software. Fig. 3 shows an example of 3D-reconstruction images obtained for the C1 composite. Tab. 2 shows the volume fractions of the constituents obtained for the two composites, C1 (with a high binder content) and C2 (with a low binder content).



Fig. 2. Nanotom tomograph with a straw composite sample

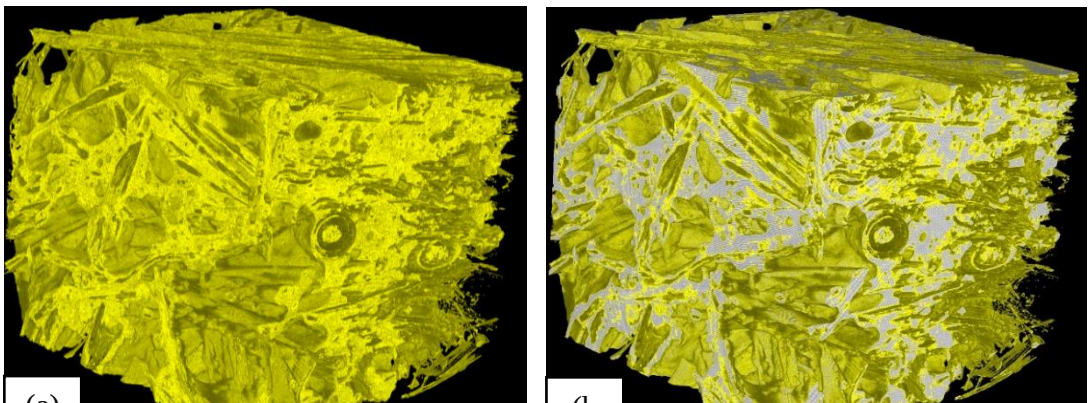


Fig. 3. 3D-reconstruction of a straw concrete sample (a) straw (b) combination straw and binder (c) composite (straw+binder+porosity).

	C1	C2
Binder	33%	11%
Straw	30%	35%
Porosity (intergranular)	37%	54%

Tab. 2 . Volume fractions of the different phases for the two composites

2.2.2 Thermal and mechanical characterization

To evaluate the experimental mechanical behavior of the two composites, uniaxial compression tests were carried out using a compression testing machine (IGM250), equipped with a load cell of 25 kN at a displacement rate of 0.5 mm/min. It should be noted that during the manufacture of composites, under the effect of the self-weight of the mixture, the straw aggregates tend towards stratified planes perpendicular to the compaction direction (Fig. 4). For this reason, the tests were carried out in the perpendicular direction to compaction (horizontal) on 20 × 20 × 10 cm^3 samples (Fig. 5-a) and also in the parallel direction of aggregates (vertical) on 15 × 15 × 10 cm^3 samples (Fig. 5-b).

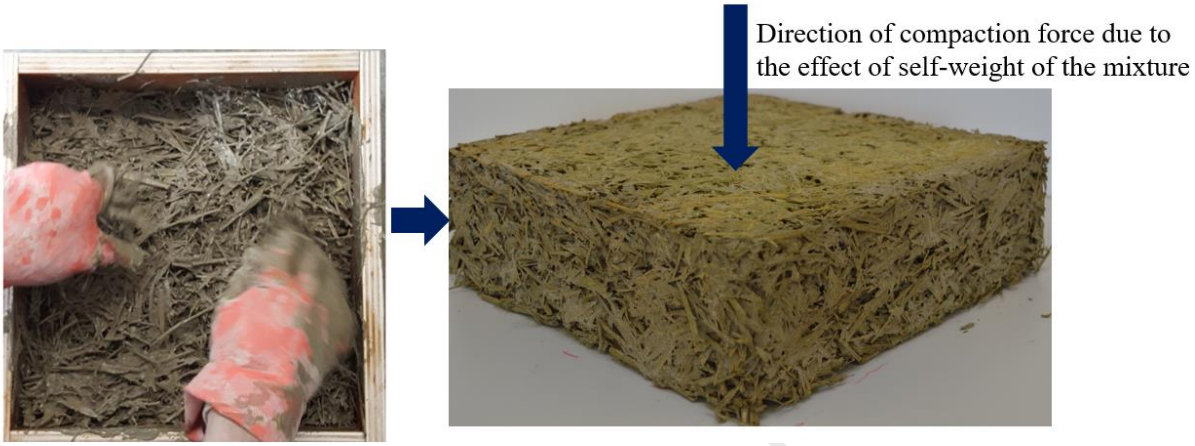


Fig. 4. Direction of compaction due to the self-weight of the mixture

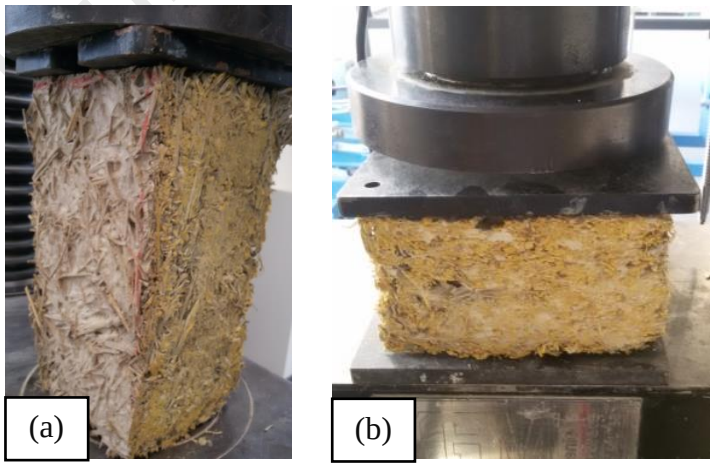


Fig. 5. Uniaxial compression test (a) horizontal direction (b) vertical direction

Thermal conductivity was measured using a NeoTIM conductivity meter based on the hot wire technique. The measurements were made on samples with the dimensions 20 cm × 10 cm × 10 cm in horizontal (Fig. 6a) and vertical direction (Fig. 6b). The probe was placed in

five different positions and the test was repeated three times in each position. The test was carried out in a dry state (the composites were dried in a ventilated oven at 60 °C until mass stabilization).

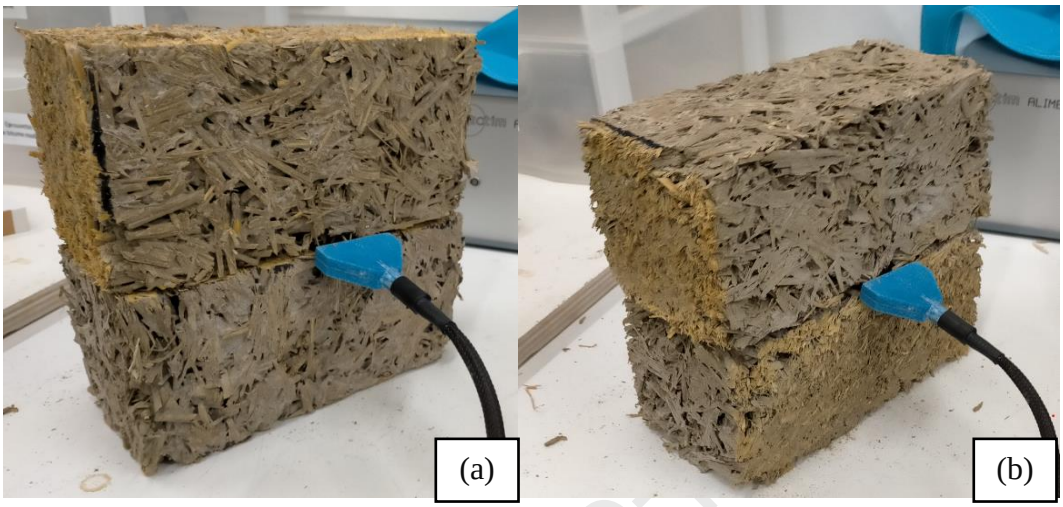


Fig. 6. Thermal conductivity measurement (a) horizontal direction (b) vertical direction.

The thermal and mechanical characterization carried out in the horizontal and vertical direction highlighted the effect of the aggregate's orientation on the behavior of the materials. Fig. 7 shows a comparison between the stress-strain curves evaluated from the uniaxial compression tests on the composites studied in both directions. The mechanical behaviour obtained in the horizontal direction is similar to what is observed for hemp concrete [36]. The curve has three zones: an elastic zone, where the binder supports the compressive stress, a nonlinear zone depicting the progressive cracking of the binder until failure, and a post peak zone where the binder is totally damaged and the vegetal aggregate supports most of the stresses. Contrary to the horizontal direction, the loading of the composites in the vertical direction results a behavior which is characterized by the absence of a fracture peak (Fig.7b), the curve shows a continuous compaction with increase of the stress with large strain.

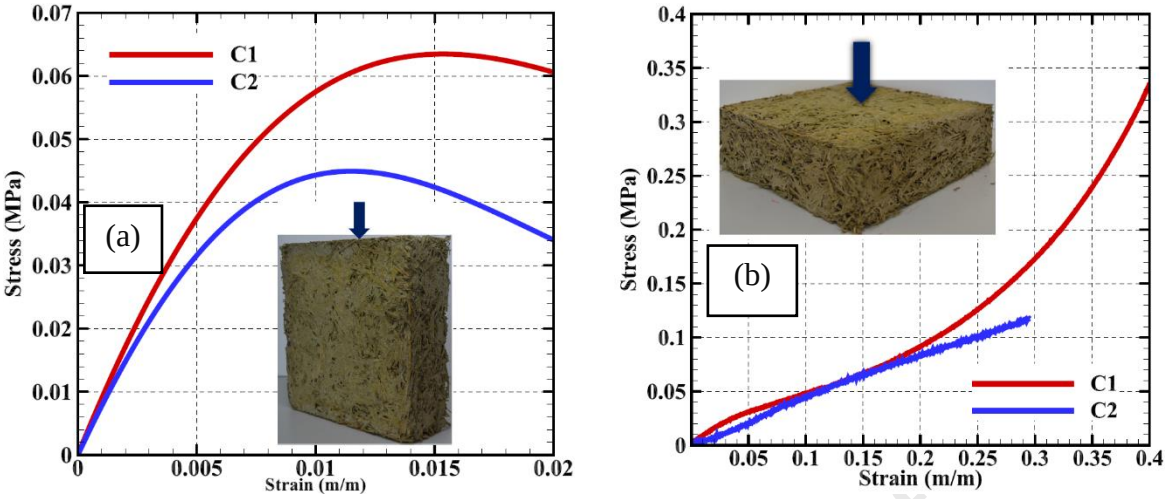


Fig.7 . Mechanical behavior of composites (a) horizontal direction (b) vertical direction.

A difference in thermal conductivity was also noted in both directions. The values measured in the vertical direction are higher than those obtained in the horizontal direction for both composites as presented in Tab.3.

These results show that the fibre orientation strongly influences the properties of the composites and leads to a transverse isotropy of the materials [30].

	Thermal conductivitiy (λ/W/m.K)	
Composites	Vertical direction	Horizontal direction
C1	0.075±0.02	0.064±0.013
C2	0.057±0.017	0.051±0.019

Tab.3 . Thermal conductivity of composites in horizontal and vertical direction

2.2.3 Distribution of fiber aspect ratio

Fig.8 show the results of the distribution of fiber aspect ratio obtained from the granulometric analysis of aggregates [35], it can be seen that more than 75% of the aggregates have an aspect ratio in the range of 3-7, with the largest percentage being assigned to aspect ratio in the interval]4 ;5].

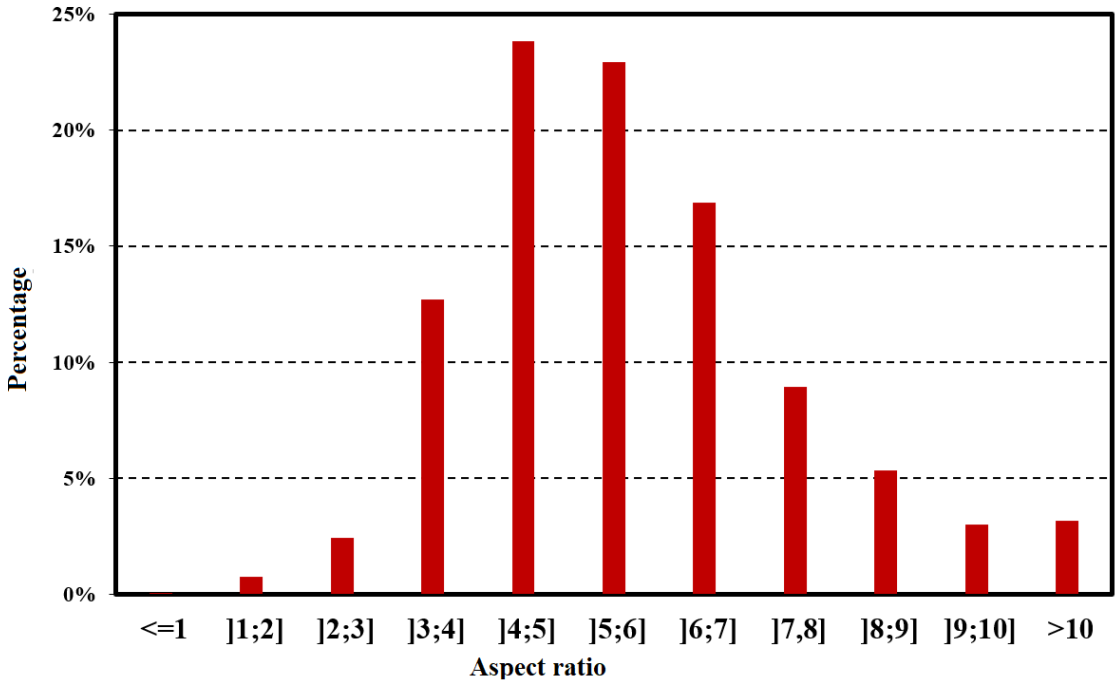


Fig. 8. Distribution of aspect ratio of aggregates used for the manufacture of composites.

3 Modeling of thermal conductivity and nonlinear mechanical behavior

3.1 Conceptual model of the microstructure of the biocomposites

The microstructural information obtained from the experimental characterization described in the previous section was used to create a three-dimensional microstructure using the Digimat software. The straw aggregates were represented by curved sphero-cylindrical inclusions (Fig. 9a) with a constant aspect ratio equal to 4 and the porosity (intergranular porosity or straw porosity) was represented by spherical inclusions (Fig. 9b) randomly distributed. Also, in order to take into account the anisotropy demonstrated in previous section, the sphero-cylindrical inclusions were randomly oriented in the plane (2D) (Fig. 10).



(a) (b)

Fig. 9. Shapes of inclusion adopted for (a) straw (b) Porositiy

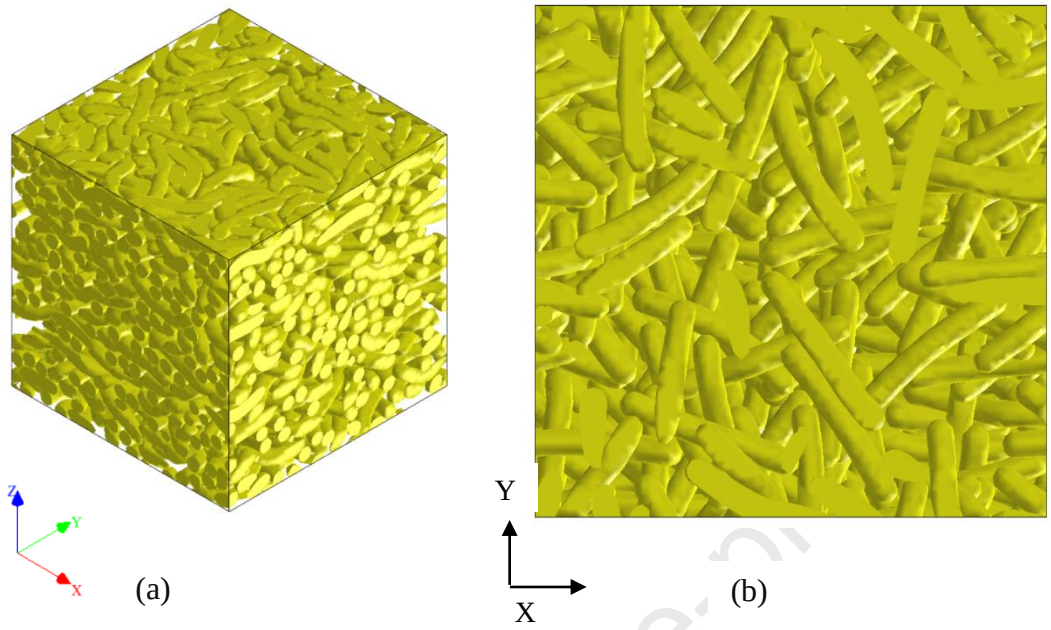


Fig. 10. Example of a RVE showing the random orientation in the plane of inclusions.

In order to highlight the influence of the microstructure on the effective thermal conductivity of the biocomposites, five different configurations of the conceptual model of the biocomposite microstructure have been adopted:

Configuration 1: It consists of introducing the heterogeneities of the material in two successive steps. First, the binder and porosity were homogenized. Then, the obtained equivalent homogeneous medium (EHM), constituted the matrix in the second step, while the straw inclusions were integrated to determine the effective conductivity of the final homogenized material (Fig. 11).

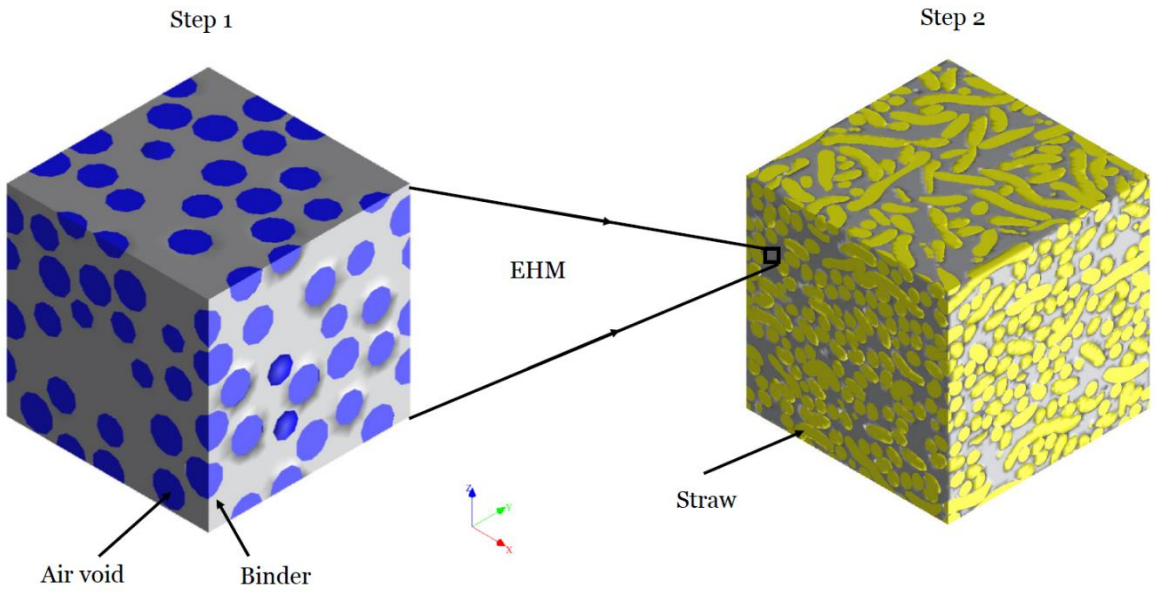
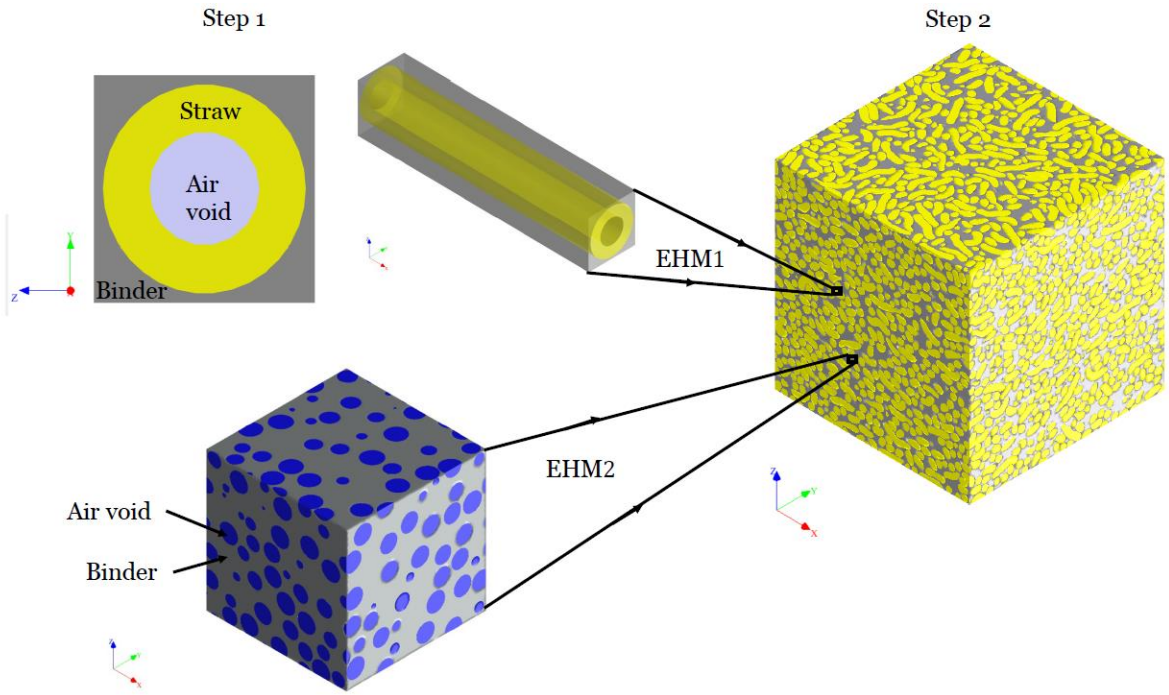


Fig. 11. Microstructure used in configuration 1

Configuration 2: The binder has been divided into two parts: a large part (95%) that coats the fibers and another part (5%) that provides the bonding bridges (porous binder) between them. Therefore, the heterogeneities were represented by a tri-composite inclusion containing the air surrounded by the straw and itself coated with the layer of binder. Then, a two-step homogenization was also adopted: the first step consists in determining separately the effective thermal conductivity of the tri-composite inclusion (air + straw + binder) and the porous binder. Then for the second step, the RVE contain the two homogeneous media determined in the first one to obtain the final effective behavior (Fig. 12).

Journal Pre-proof



290
291 **Fig. 12.** Microstructure used in configuration 2

292

293 Configuration 3: we assume in this case that the material consists of a network of fibers
294 coated by the binder and embedded in the void matrix. The process consists in a first step in
295 determining the effective thermal conductivity of a bi-composite inclusion representing the
296 straw coated by the binder. Then, this conductivity will be assigned to heterogeneities
297 immersed in a matrix completely represented as a void and a second homogenization was
298 carried out. Note that the contact between the binder and the straw is considered as perfect
299 (Fig. 13).

Journal Pre-proof

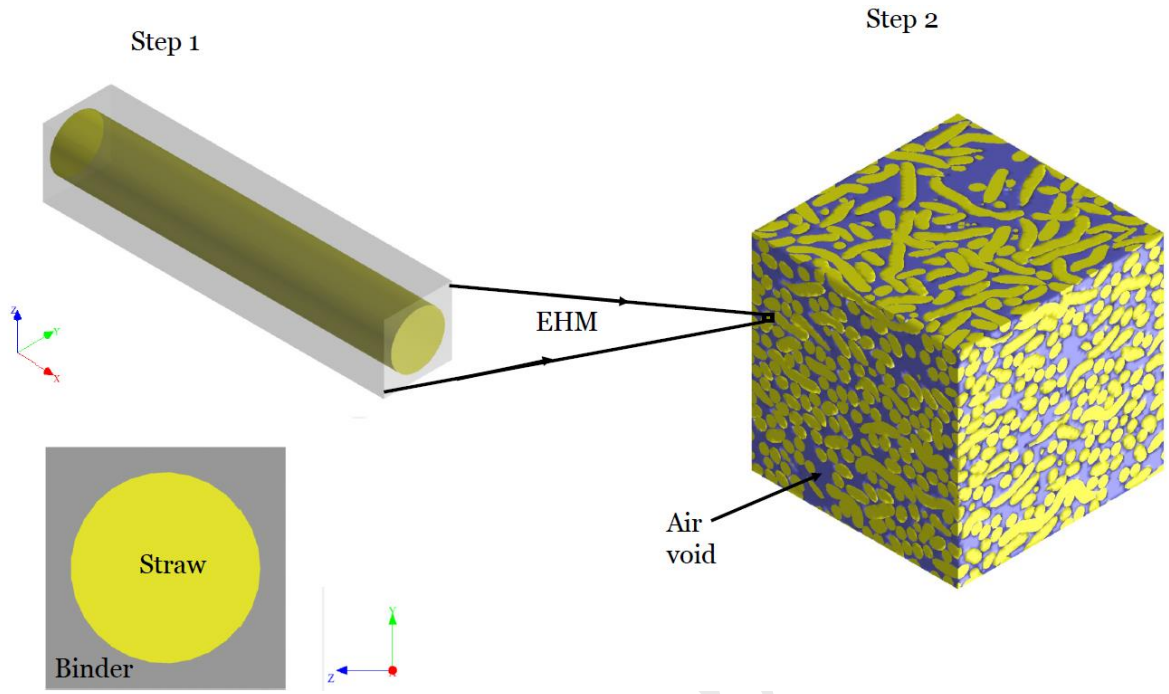


Fig. 13. Microstructure used in configuration 3

Configuration 4: Similar to the second configuration, the binder was divided into two parts, a 95% percentage that coats the fibers and another 5% which connects the fibers with each other. In a first step, the equivalent homogeneous medium of the bi-composite inclusion and the porous binder were determined, then in a second step, the two equivalent homogeneous mediums were integrated in an RVE where the matrix represents the porous binder and the heterogeneities represent the coated straw. A perfect interface was also considered in this case (Fig. 14).

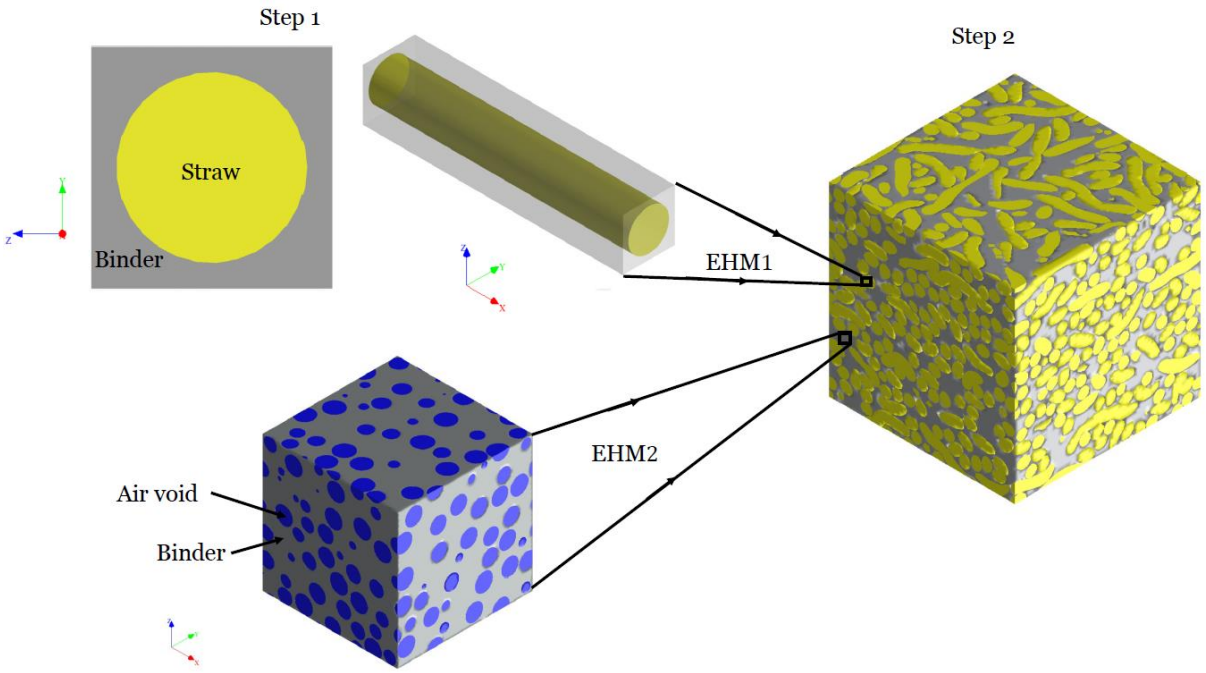


Fig. 14. Microstructure used in configuration 4

Configuration 5: The same previous approach was followed in this configuration but an inter-phase between binder and straw was introduced. The properties of this zone were determined by calibrating the numerical model on the experimental results. As for its thickness, it is assumed to be very small compared to the diameter of inclusion (interphase thickness≃1% of diameter of inclusion) (Fig. 15).

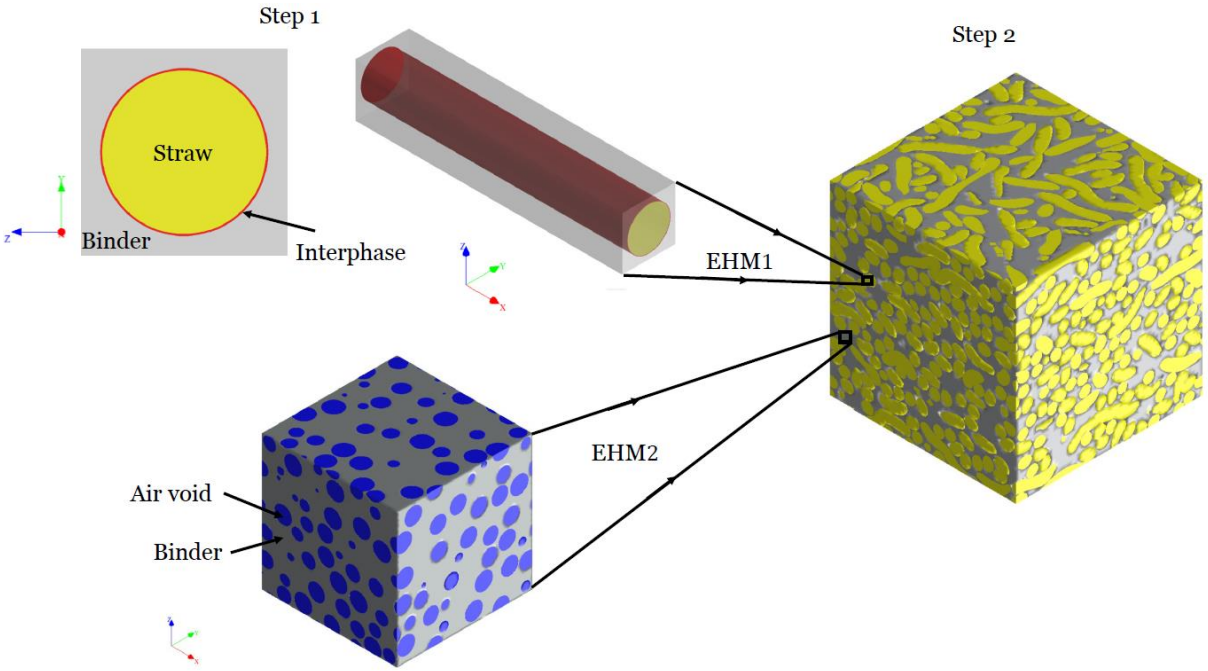


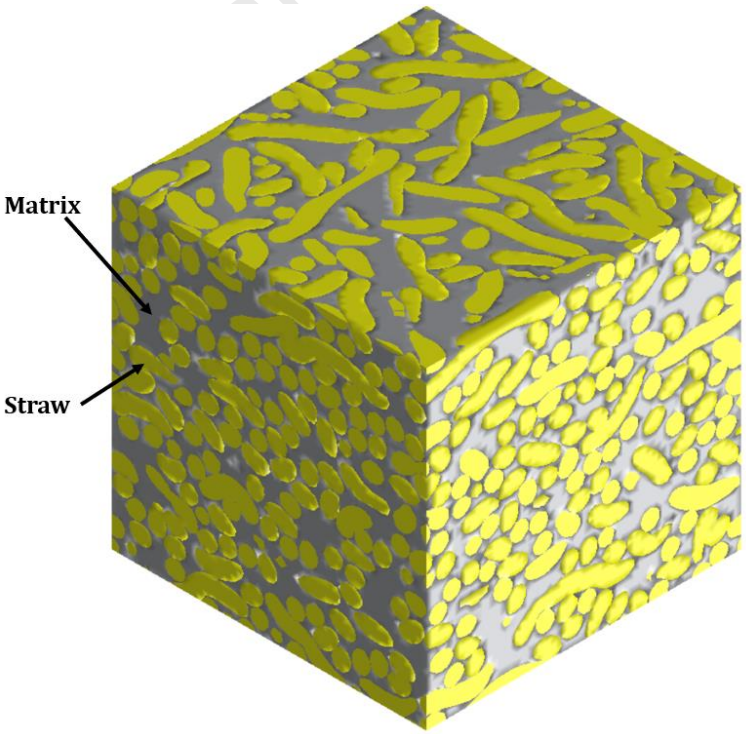
Fig. 15. Microstructure used in configuration 5

3.2 Size of the representative Volume Element (RVE)

The relevant choice of a representative volume element (RVE) is the first step to accurately describe the microstructure of the material to be modelled. Several approaches have been proposed in the literature to determine its size. According to Hill.1963 [37], the RVE is a sample which contains sufficient heterogeneities for the macroscopic properties to be independent of the boundary conditions. Hashin.1983 [38] indicates that the RVE must be large enough in relation to the scale of the heterogeneity and small enough in relation to the macroscopic scale of the composite material. Kanit et al. 2003 [39], Gitman et al. 2007 [40], Pelissou et al. 2009 [41] proposed a statistical analysis based on the convergence of the effective properties to set the size of the representative volume. Indeed, the approach consists in estimating the apparent properties of the material by performing several numerical calculations on different sizes of the microstructure containing the same volume fraction of the heterogeneities and under the same boundary conditions. The size of the micro-structure

335 from which the apparent properties converge corresponds to the size of the Representative
336 Volume Element (RVE).

337 A similar approach is used here to determine the RVE size of straw composite in the thermal
338 and mechanical case. We consider five sizes of a cubic RVE whose dimension of the edge is
339 between 1 and 3 cm. We aim to determine for each size the effective thermal conductivity as
340 well as the Young's modulus. We also consider that the RVE contains a single form of
341 inclusion (curved sphero-cylindrical inclusions) with constant size and randomly oriented in
342 the plane (Fig.16). Five simulations were carried out for each size to determine the standard
343 deviation of the estimated parameters. The approach was applied for two volume fractions of
344 inclusions: 25% and 60%. The simulations and the generation of the microstructure were
345 carried out using the Digimat software. A set of parameters given in table 4, for lime matrix
346 and straw inclusion is used for all simulations.



347

348 **Fig. 16.** Microstructure used to determine the RVE size

349

	Matrix	Inclusion
Young's modulus E(MPa)	100	0.2
Poisson's ratio ν	0.3	0.1
Thermal conductivitiy (λ/W/m.K)	0.168	0.051

Tab. 4. Parameters used to determine effective properties.

Fig. 17 shows the evolution of thermal conductivity and Young's modulus as a function of the edge size of RVE for the two volume fractions considered. We can notice in the thermal case that the effective conductivity converges from a size of 2 cm for a volume fraction of 25% while for a fraction of 60% the convergence is shifted to a size of 2.5 cm.

In the case of Young's modulus, for a fraction of 25% the convergence was observed in the vicinity of 2.5 cm while for a percentage of inclusions of 60%, it is reported at a size of 3 cm. We can also note that in the different cases, the standard deviation decreases as the size of the RVE increases.

These results show that the size of the RVE can depend on the volume fraction of the heterogeneities in both linear elasticity and heat conduction. According to these results, a representative cubic volume element with an edge of 3 cm was adopted to estimate the thermal conductivity and the mechanical behavior of the studied straw composites. We note that the average straw size is about 2.9 cm, determined from granulometric analysis of studied particles [35]. However, to reduce the computation time of the simulations, we used in the conceptual model of the microstructure an inclusion with an average size of about 1 cm which allows to have a same ratio of 3 between the size of the inclusion and the RVE edge.

Journal Pre-proof

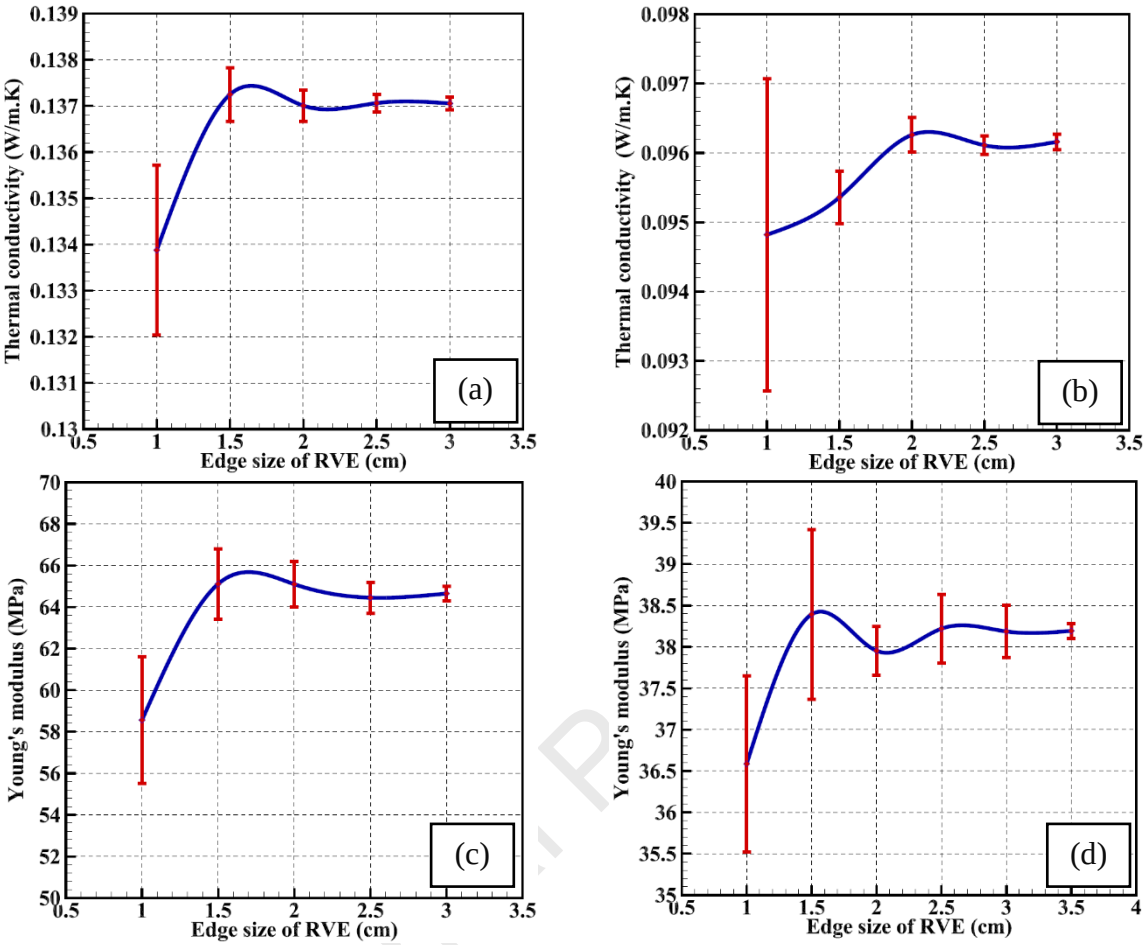


Fig. 17. Variations of the effective apparent properties as a function of the edge size of the RVE: (a) and (b) Thermal conductivity respectively for a fraction of 25 % and 60%; (c) and (d) Young's modulus respectively for a fraction of 25% and 60%

3.3 Modeling of thermal conductivity

As it was described above, we consider a cubic RVE with an edge of 3 cm, composed of a matrix and two types of inclusions: spherical representing the porosity (inter-granular and tubular pore of straw) and curved sphero-cylindrical corresponding to the vegetable aggregates. Tab. 5 shows the input data used for the three components. The thermal conductivities given for the matrices were measured on samples of the binder pastes using the hot wire method. The numerical simulations were performed using a Digimat software. A temperature difference of 20°C was imposed between two opposite hot and cold faces and periodicity boundary conditions on the other faces (Fig. 18). The thermal loading was applied

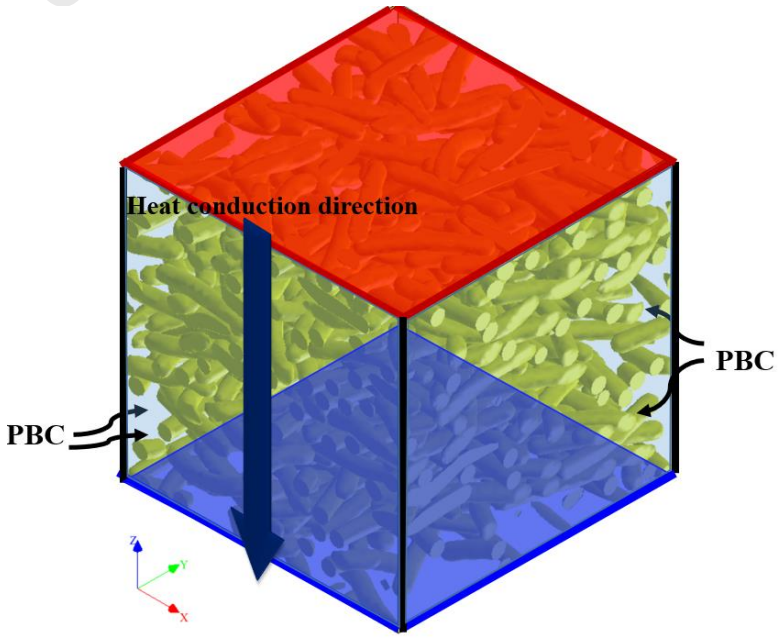
in the perpendicular direction in order to compare the numerical results with the experimental measurements. A tetrahedral mesh was used in simulations because of its flexibility in modelling complex 3D geometries (Fig. 19). The effective thermal conductivity (λ_{eff}) is calculated as:

$$\lambda_{eff} = \frac{q_h}{\Delta T} \quad (1)$$

where q_h is volume-averaged heat flux in the RVE along the Z-direction and ΔT is the imposed temperature difference.

Constituents	Thermal conductivity (W/m.K)
Matrix of C1-composite	0.168
Matrix of C2-composite	0.143
Straw	0.051
Air	0.026

Tab. 5. Thermal conductivities of constituents



Journal Pre-proof

Fig. 18. Direction of thermal conduction between hot and cold sides and periodic boundary conditions (PBC) imposed on the other faces.

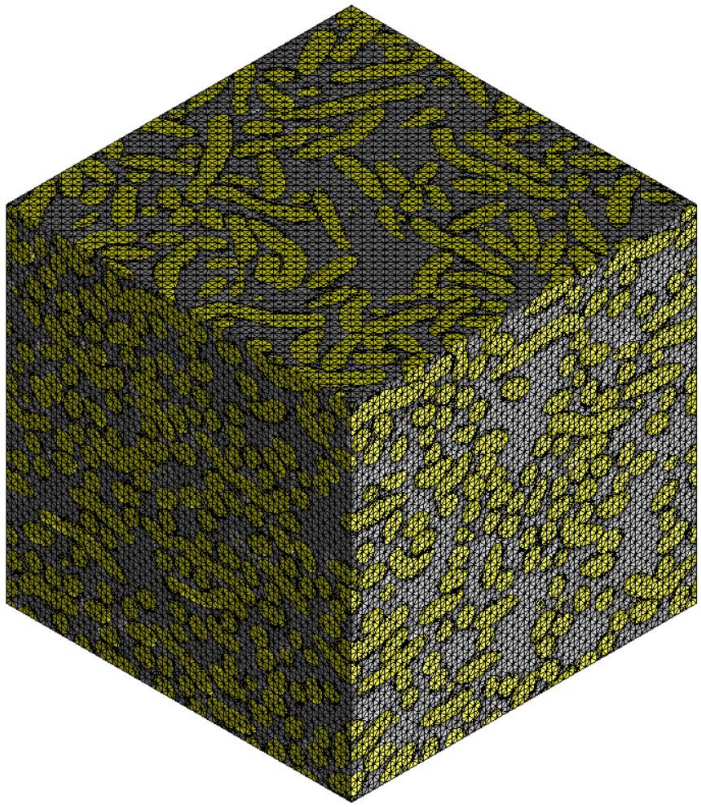


Fig. **19.** Three-dimensional mesh of the RVE using tetrahedral elements.

Fig. 20 shows the results obtained in the different configurations presented above. It appears that the classical representation of the microstructure by inclusions embedded in a matrix with perfect interface between the matrix and the inclusion, provides results is far away from those obtained experimentally with an error of about 20% for the two biocomposites.

The microstructure adopted in the second configuration has improved the obtained numerical results. Indeed, the numerical values are close to those obtained experimentally, the relative errors are of the order of 4.13% and 7.03%, respectively for the composite with a high and low binder content. Moreover, the third proposed configuration by introducing coated fibers in a void volume has largely underestimated the thermal conductivity of the materials with an error of up 30 % for the C2 biocomposite. However, the replacement of this matrix (void) by

a porous matrix allowed satisfactory results, particularly for the low-dosage composite C2. Finally, considering another phase between the binder and the matrix allowed to reproduce faithfully the experimental results in the case of both composites.

We can confirm from these results the significant impact of the choice of microstructure on the estimation of the effective thermal conductivity of materials. Indeed, although the volume fractions of the three phases of the material are the same in the five configurations considered, the results were very variable. This result confirms that the effective properties of heterogeneous material depend not only on the properties of the constituents but also on their interactions represented by the different conceptual models of the microstructure. Therefore, choosing a microstructure close to that of the real material is an essential step to be able to accurately predict the effective thermal conductivity.

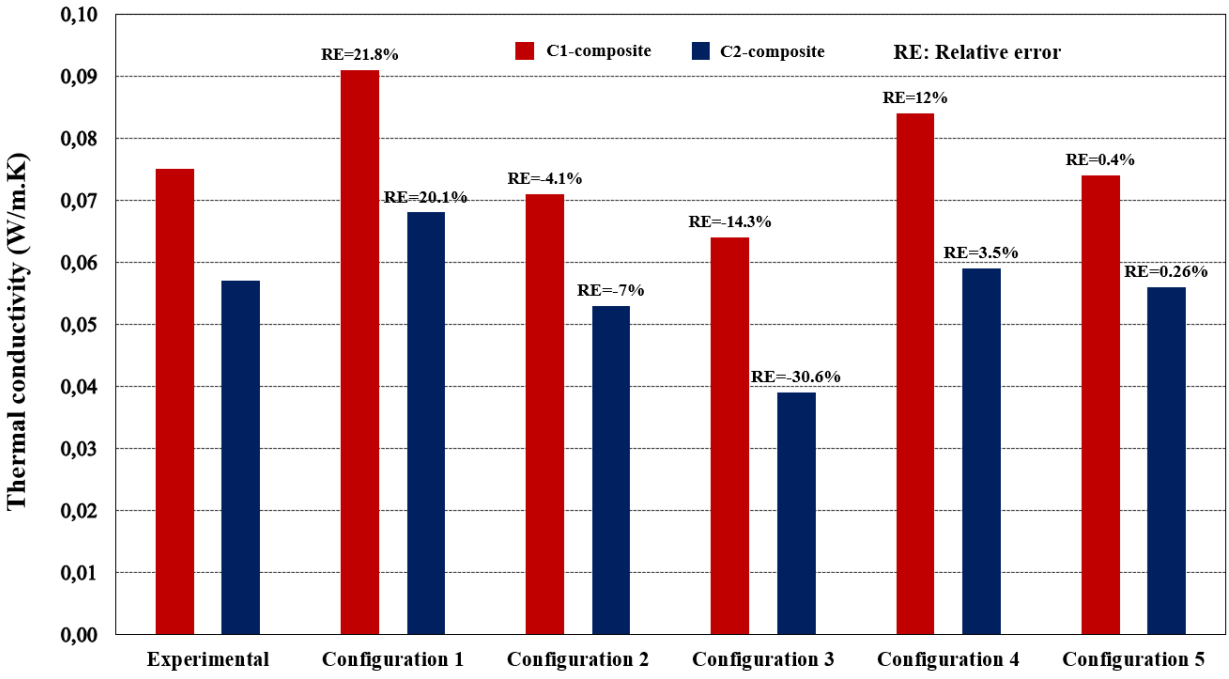


Fig. 20. Comparison between experimental and modelled thermal conductivities.

3.4 Modeling of the nonlinear mechanical behavior

Numerical homogenization was also used to reproduce the mechanical behavior of the two studied straw composites. As well as the problem of heat conduction, a representative volume element is considered, which consists of elastic heterogeneities and an elastoplastic matrix. Two shapes of inclusion were adopted, spherical representing the porosity (inter-granular and tubular pore of straw) and curved sphero-cylindrical corresponding to the vegetable fibres. The boundary and loading conditions were imposed on the surfaces as shown in the Fig. 21.

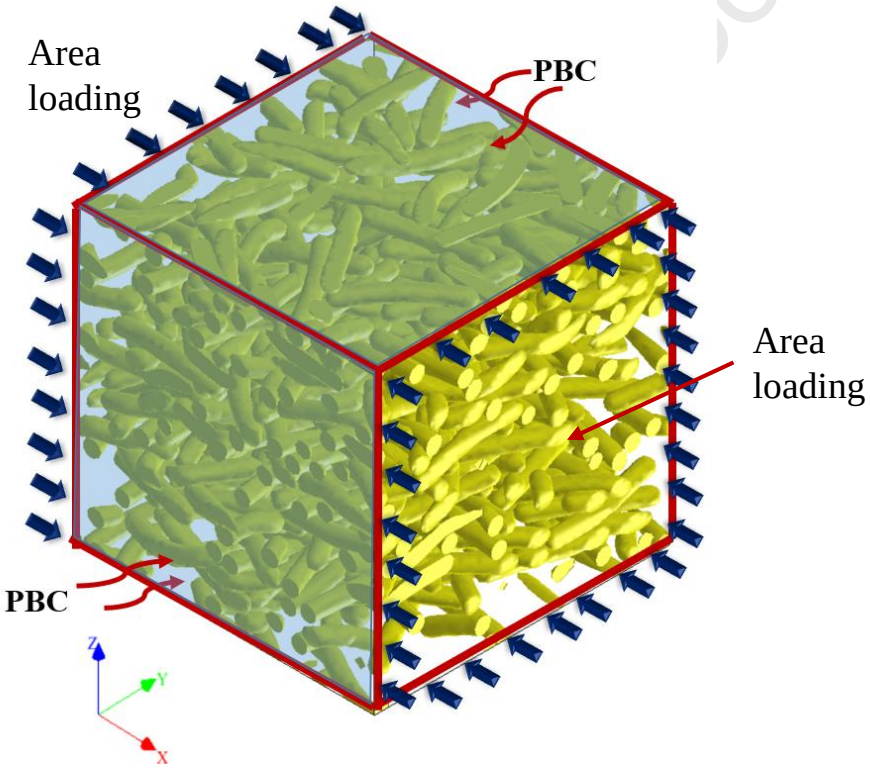


Fig. 21. Direction of mechanical loading and periodic boundary conditions (PBC) imposed on the other faces.

Tab. 6 gives the elastic properties of the inclusions used in the simulations.

	Straw	Air void
Young's modulus E (MPa)	0.2	10^{-6}
Poisson's ratio ν	0.1	0.001

442

443 **Tab.6 .** Elastic parameters of the inclusions (Straw + air)

444 The behavior of the matrix is described by a J_2-plasticity model with nonlinear isotropic

445 hardening. This model is based on the Von Mises equivalent stress σ_{eq} defined as :

$$\sigma_{eq} = \sqrt{J_2(\boldsymbol{\sigma})} = \sqrt{\frac{3}{2}(\boldsymbol{s}:\boldsymbol{s})} \tag{2}$$

446 where $J_2(\boldsymbol{\sigma})$ is the second invariant of the deviatoric stress tensor **s**, and is expressed as:

$$\begin{aligned} J_2(\sigma) &= \tfrac{3}{2}(\boldsymbol{s}:\boldsymbol{s}) \\ &= \frac{2}{3}\left[(\boldsymbol{\sigma} - \frac{1}{3}Tr(\sigma)\boldsymbol{I}\right]:\left[(\boldsymbol{\sigma} - \frac{1}{3}Tr(\boldsymbol{\sigma})\boldsymbol{I}\right] \\ &= \tfrac{1}{2}[(\sigma_{11}-\sigma_{22})^2 + (\sigma_{22}-\sigma_{33})^2 + (\sigma_{33}-\sigma_{11})^2] + 3[(\sigma_{12}^2 + \sigma_{23}^2 + \sigma_{31}^2)] \end{aligned} \tag{3}$$

447 In this constitutive model, the response is assumed to be linear elastic as long as the following

448 condition is satisfied:

$$\sigma_{eq} \leq \sigma_Y \tag{4}$$

449 where σ_Y is the initial yield stress.

450 The total strain is assumed to be the sum of the plastic strain and elastic strain:

$$\boldsymbol{\epsilon} = \boldsymbol{\epsilon^e} + \boldsymbol{\epsilon^p} \tag{5}$$

451 The Cauchy stress and the elastic strain are then related by :

$$\boldsymbol{\sigma} = \underline{\underline{\mathbf{C}}}:(\boldsymbol{\epsilon} - \boldsymbol{\epsilon^p}) \tag{6}$$

452 where $\underline{\underline{\mathbf{C}}}$ is Hooke's operator. When σ_{eq} exceeds σ_Y, the response becomes nonlinear and

453 plastic deformation appears. In this case, the Cauchy stress is given by

$$\sigma_{eq} = \sigma_Y + R(p) \tag{7}$$

454 where R(p) is the hardening stress expressed by a exponential and linear law:

$$R(p) = kp + \sigma_\infty[1 - \exp(-mp)] \quad (8)$$

455 Where k : is a linear hardening modulus, σ_∞ : is a hardening modulus, m : is a hardening
456 exponent and p the accumulated plastic strain, expressed as,

$$p(t) = \int_0^t \dot{p}(\tau)\ d\tau \quad (9)$$

457 With

$$\dot{\mathbf{p}} = \frac{2}{3}\sqrt{J_2(\dot{\boldsymbol{\epsilon}}^{\mathbf{p}})} = \sqrt{\frac{2}{3}\dot{\boldsymbol{\epsilon}}^{\mathbf{p}} : \dot{\boldsymbol{\epsilon}}^{\mathbf{p}}} \quad (10)$$

458 A yield function f (σ,R) can be defined,

$$f(\sigma, R) = \sigma_{eq} - \sigma_Y - R(p) \leq 0 \quad (11)$$

459 If f (σ,R)≤0, the material evolves in the elastic domain. Otherwise it is in the plastic region.
460 The evolution of the plastic strain tensor ε^p is given by the normality rule :

$$\dot{\boldsymbol{\epsilon}}^{\mathbf{p}} = \dot{\mathbf{p}}\frac{\partial f}{\partial \sigma} \quad (12)$$

461 To determine the parameters (σ_Y,σ_∞, k, m) of the micromechanical model, uniaxial
462 compression tests were carried out on binder pastes for each case, Fig. 22 illustrates the stress-
463 strain curves obtained for the two matrices and Tab. 7 shows the parameters identified from
464 these curves.

Journal Pre-proof

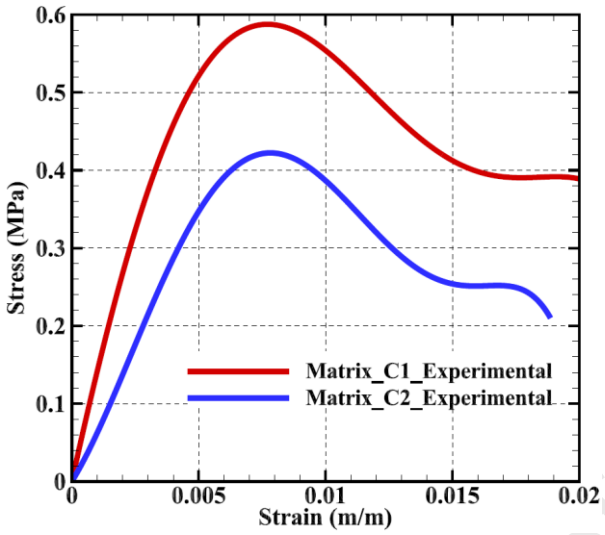


Fig. 22. Mechanical behavior of pure binders

	Matrix_C1	Matrix_C2
Poisson's ratio ν	0.3	0.3
Young's modulus E(MPa)	100	85
Limite d'élasticité σ_Y (MPa)	0.25	0.09
Hardening modulus σ_∞ (MPa)	0.38	0.37
Hardening exponent m (MPa)	1400	1396
Linear hardening modulus k (MPa)	-5.5	-3.8

Tab. 7 Parameters used for the mechanical modelling

The mechanical behavior of the two composites was estimated by following the steps of configuration 1 (Fig. 11). First, the spherical inclusions and the matrix were homogenized. Then, in a second step, the curved fibers were integrated in the equivalent medium determined in the first step and a new homogenization is performed to obtain the effective mechanical behavior of the composite. The simulations were carried out by imposing on one face of the RVE a uniaxial deformation (in the x-direction, Fig. 21) and periodic conditions in the other faces. A tetrahedral mesh was also used here in both calculation steps.

Fig. 23 compares the experimental stress-strain curves with those predicted by the numerical homogenization. The numerical curves are well above the experimental ones in both the

elastic and plastic region. This discrepancy can be associated with the matrix input data, evaluated from the compression tests on binder pastes alone. In other words, the behaviour of pure binders may be different from that of binders mixed with fibres, leading to significant errors. The binder alone has a compactness that is totally different in the presence of aggregates. This problem was also discussed by Akkaoui et al. 2017 [28]. Indeed, to determine the elastic properties of the constituent phases of wood concrete, the authors carried out a calibration of the developed model on the experimental results of the composite. They noticed that the calibrated modulus arelower than those measured on the pure binder paste. This difference is due to the interactions between the plant fibers and the binder. The presence of the fibers strongly impacts the hydration and drying process of the binder [42–44]. In addition, the cracks that appear in certain area of the fiber-matrix interfaces lead to additional porosity which can also be the cause of the weakness of the calibrated properties for the binder.

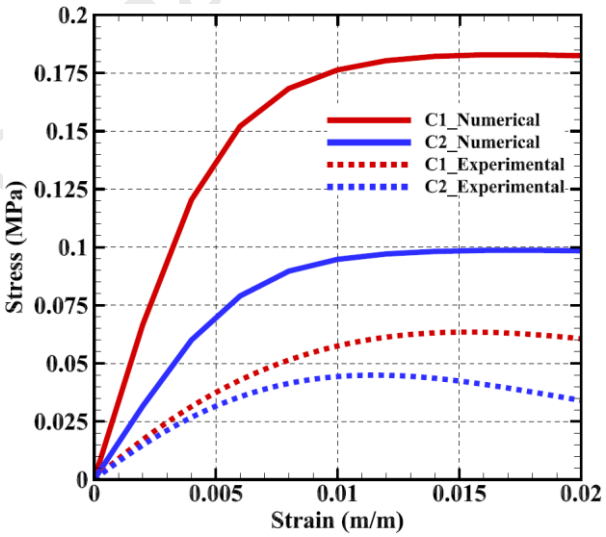


Fig. 23. Modeled and experimental mechanical behavior of the two composites

Therefore, we propose to determine the behavior of the matrix using an inverse analysis based on numerical homogenization. For this, we assume the following hypotheses: (i) The representative volume element is cubic with an edge equal to 3 cm (ii) Vegetable fibers have a curved sphero-cylindrical shape, randomly oriented in the plane and they have the same

aspect ratio (iii) Porosity has a spherical shape (iv) The behavior of the inclusions is elastic as shown in the Tab. 8. (v) The behavior of the matrix is elastoplastic. The macroscopic stresses and strains are calculated from the mean relations of the local stresses and strains of the RVE. We aim to evaluate the properties of the matrix (parameters of J2-plasticity model). In a first step, we determine the elastic properties of the matrix allowing to minimize the difference between the experimental and numerical curve by using least squares. Once this condition is satisfied, we fix the elastic parameters and we proceed to determine the plastic parameters (σ_Y,σ_∞, k, m) of the J2-plasticity model using the same algorithm.

Fig. 24(a) shows a good agreement between the effective behavior and that obtained from the experimental tests, whether for the composite with high or low binder content. In fact, the Young's modulus and the estimated mechanical strengths are very close to the experimental values, the standard deviation does not exceed 3%. Fig. 24(b) shows the stress-strain curves deduced from the compression tests on pure binders and those obtained by inverse analysis. This result confirms the major impact of plant fibres on the reduction of the mechanical properties of the matrices.

The approach proposed in this study can be used to orient the formulations of studied materials by proposing composites suitable for each use with a well-defined criterion.

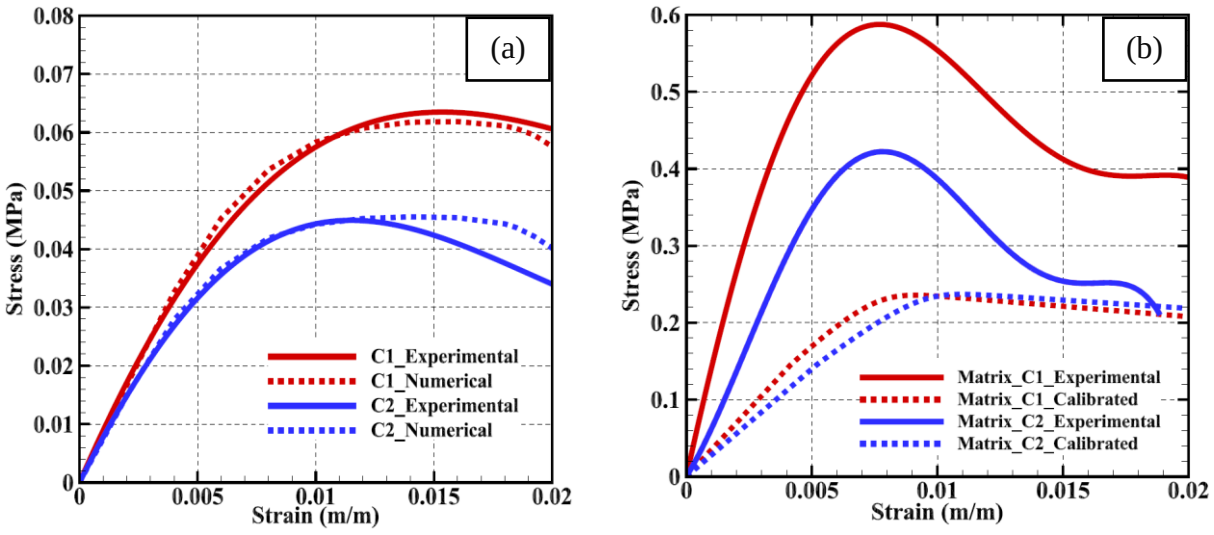


Fig. 24. Calibrated and experimental mechanical behavior (a) composites (b) matrices

	Matrix_C1	Matrix_C2
Poisson's ratio ν	0.3	0.3
Young's modulus E(MPa)	30	35
Limite d'élasticité σ_Y(MPa)	0.15	0.145
Hardening modulus σ_∞ (MPa)	0.098	0.097
Hardening exponent m (MPa)	1800	1795
Linear hardening modulus k (MPa)	-2.9	-2.5

Tab. 8 Parameters used for the modeling of the mechanical behavior

4 Model application and discussion

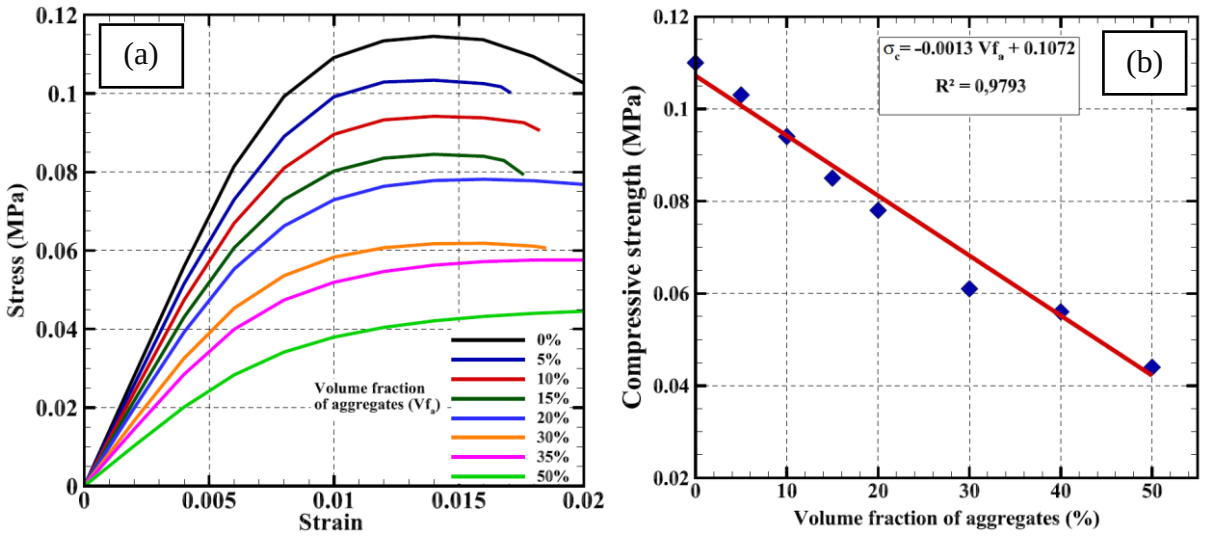
As previously mentioned int the state of the art section, the characterization of biobased materials, has shown that their macroscopic properties are closely related to the manufacturing parameters, such as, the nature and fraction of the binder, the nature and fraction of the aggregates, the size of the aggregates, and the casting process (compaction) which strongly influences the orientation of the aggregates. Other works in the literature have also shown the great sensitivity of the thermal conductivity to moisture content of the material [22–24].

The numerical model proposed in this work represents a good tool which could be used to optimize the properties of these materials as a function of physical properties of the components and microstructural description.

Among the manufacturing parameters of biocomposites that this proposed modelling will be able to give is the proportions of components or component volume fraction of the binder, the aggregates and the porosity. Fig. 25 shows an example of the results obtained by the model on the variation of thermal and mechanical properties of C1-composite as a function of volume fraction of the aggregates (Vfa).

Numerical simulations were performed using the microstructure described in configuration 1 (Fig. 11). In the first step, the binder and porosity were homogenized and in the second step several volume fractions (between 5% and 50%) of the aggregates were tested and

homogenized. These simulations were carried out using the VERs and the boundary conditions presented previously in the figures 18 and 21. Fig.25-a shows the variation of the mechanical behavior of the composite as a function of the volume fraction of the aggregates. It is clear that the stress strain curves become more ductile with the increase in volume fraction of the aggregates. As expected, the more this fraction of the aggregates decreases, the more the behavior of the composite becomes close to that of the matrix. Similar results were obtained by Arnaud et al. 2012 [21] for the hemp concrete. Moreover, as displayed in Fig. 25-b and 25-c, a quasi-linear correlations were found between the mechanical properties and the volume fraction of the aggregates. The compressive strength and Young's modulus decrease proportionally with increasing percentage of aggregates. These results are in agreement with the results found by Akkaoui.2015 [45] for wood-aggregate concrete, Mazhoud et al. 2017 [46] for hemp clay composite, and Pham 2014 [27] for hemp concrete. Fig. 25-d also shows a quasi-linear evolution between the thermal conductivity and the volume fraction of the aggregates. As known, the increase in percentage of aggregates leads to a decrease in thermal conductivity. The same trend was obtained also by Cerezo.2005 [25], Tran-Le et al. 2018 [29] and Pham.2014 [27] that used analytical models to predict the thermal conductivity of hemp concrete.



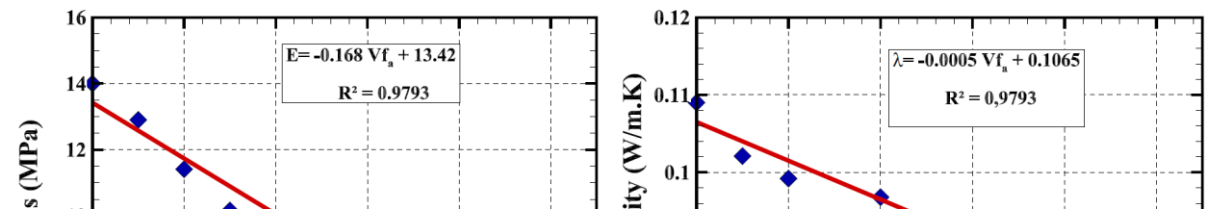


Fig. 25. Variation of mechanical and thermal properties as a function of volume fraction of the aggregates (Vf_a) (a) nonlinear mechanical behavior (b) Compressive strength (c) Young modulus (d) thermal conductivity

The use of the modelling approach presented here can make it possible to propose optimal mixtures with an attractive thermal and mechanical properties depending on the final applications and the criteria for use in buildings. The numerical modelling is able to predict the stress-strain curve of the materials and to estimate their mechanical strength even for high fraction of aggregate unlike analytical models used in literature which are limited only to fractions not exceeding 30 %. Despite the advantage of this promising modelling method that allows to study complex microstructures, the proposed methodology is based on some assumptions that affect certain results. The first, is that the mechanical properties of the binder is determined by inverse analysis assuming that the volume fraction of the aggregates in composite is constant. The variation of aggregate fraction can impact significantly the intrinsic characteristics of the matrix due to the interactions between the plant aggregates and the binder as we previously stated. Therefore, it will be interesting to evaluate the influence of plant aggregates on the intrinsic properties of the matrix. Moreover, the aggregate-matrix interface is assumed to be perfect. This assumption is not realistic as it has been shown by the microscopic observation. The experimental characterization of this interface and its

Journal Pre-proof

591 consideration in the material modelling in terms of thickness and properties has not yet
592 reached a complete consensus, and remains an important point of investigation.
593

594 5 Conclusion
595

596 The purpose of this paper was to model the thermal and mechanical behavior of two types of
597 straw biocomposites. Given the limitations of the analytical methods in taking into account all
598 microstructure characteristics influencing the behavior of biobased materials, a numerical
599 homogenization was adopted in this work to model their complex behavior. First, a detailed
600 description of morphology, size and spatial distribution of inclusions was carried out. The X-
601 ray microtomography is used to determine the volume fractions of the different phases of the
602 bio-based materials. Then, a statistical approach based on the convergence of the apparent
603 properties was applied to determine the size of the representative volume element. The results
604 showed that the RVE size depends on the fraction of inclusions in the case of mechanical or
605 thermal loading. Subsequently, the effective conductivity and the non-linear behavior of the
606 composites were modeled. In the case of thermal conductivity, five configurations were
607 proposed to show the effect of microstructure on the prediction of the effective properties.
608 The obtained results have shown that the classical representation of materials by
609 heterogeneities embedded in a matrix is inappropriate for the complex materials of this study
610 contrary to the classical polymer or metallic composites with a low ratio of fibers. The
611 compressive mechanical behavior was first modeled using as input data for the matrix, the
612 parameters determined from the experimental tests on the pure binders. This led to a large
613 overestimation of the mechanical behavior. Therefore, a calibration of the numerical model
614 with the experimental curves of the composites was necessary to access the properties of the
615 matrices. The results showed that the properties determined from the experimental curves of
616 pure binders are much lower than those identified, by inverse analysis, from the curves of the

composites. These results confirm the need to consider the fiber-matrix interaction in the numerical model to accurately predict the mechanical behavior of biobased composites. However, the approach proposed in this work remains useful to guide the optimization of the mixtures design of the biocomposite materials.

6 Acknowledgements

The authors gratefully acknowledge the ‘‘REGION CENTRE” for the financial support of the research program PEPITE.

7 References

[1] S. Amziane, F. Collet, Bio-aggregates based building materials : State-of-the-Art Report of the RILEM Technical Committee 236-BBM, Springer, 2017. ISBN 9402410317

[2] N. Belayachi, M. Bouasker, D. Hoxha, M. Al-Mukhtar, Thermo-Mechanical Behaviour of an Innovant Straw Lime Composite for Thermal Insulation Applications, AMM. 390 (2013) 542–546. https://doi.org/10.4028/www.scientific.net/AMM.390.542.

[3] N. Belayachi, D. Hoxha, M. Slaimia, Impact of accelerated climatic aging on the behavior of gypsum plaster-straw material for building thermal insulation, Construction and Building Materials. 125 (2016) 912–918. https://doi.org/10.1016/j.conbuildmat.2016.08.120.

[4] M.P. Sáez-Pérez, M. Brümmer, J.A. Durán-Suárez, A review of the factors affecting the properties and performance of hemp aggregate concretes, Journal of Building Engineering. 31 (2020) 101323. https://doi.org/10.1016/j.jobe.2020.101323.

[5] Y. Jiang, A. Phelipot-Mardele, F. Collet, C. Lanos, M. Lemke, M. Ansell, A. Hussain, M. Lawrence, Moisture buffer, fire resistance and insulation potential of novel bio-clay plaster, Construction and Building Materials. 244 (2020) 118353. https://doi.org/10.1016/j.conbuildmat.2020.118353.

[6] T. Jami, S.R. Karade, L.P. Singh, A review of the properties of hemp concrete for green building applications, Journal of Cleaner Production. 239 (2019) 117852. https://doi.org/10.1016/j.jclepro.2019.117852.

[7] M.Viel, Développement de composites bio-sourcés destinés à l’isolation des bâtiments (Ph.D.thesis) Université Rennes 1. 2018

[8] P. Tronet, T. Lecompte, V. Picandet, C. Baley, Study of lime hemp concrete (LHC) – Mix design, casting process and mechanical behaviour, Cement and Concrete Composites. 67 (2016) 60–72. https://doi.org/10.1016/j.cemconcomp.2015.12.004.

[9] B. Mazhoud, F. Collet, S. Pretot, J. Chamoin, Hygric and thermal properties of hemp-lime plasters, Building and Environment. 96 (2016) 206–216. https://doi.org/10.1016/j.buildenv.2015.11.013.

[10] A. Shea, M. Lawrence, P. Walker, Hygrothermal performance of an experimental hemp–lime building, Construction and Building Materials. 36 (2012) 270–275. https://doi.org/10.1016/j.conbuildmat.2012.04.123.

[11] O. Kinnane, A. Reilly, J. Grimes, S. Pavia, R. Walker, Acoustic absorption of hemp-lime construction, Construction and Building Materials. 122 (2016) 674–682. https://doi.org/10.1016/j.conbuildmat.2016.06.106.
[12] P. Glé, E. Gourdon, L. Arnaud, Acoustical properties of materials made of vegetable particles with several scales of porosity, Applied Acoustics. (2011) 11.
[13] S. Elfordy, F. Lucas, F. Tancret, Y. Scudeller, L. Goudet, Mechanical and thermal properties of lime and hemp concrete ("hempcrete") manufactured by a projection process, Construction and Building Materials. 22 (2008) 2116–2123. https://doi.org/10.1016/j.conbuildmat.2007.07.016.
[14] S. Benfratello, C. Capitano, G. Peri, G. Rizzo, G. Scaccianoce, G. Sorrentino, Thermal and structural properties of a hemp–lime biocomposite, Construction and Building Materials. 48 (2013) 745–754. https://doi.org/10.1016/j.conbuildmat.2013.07.096.
[15] Y. Florentin, D. Pearlmutter, B. Givoni, E. Gal, A life-cycle energy and carbon analysis of hemp-lime bio-composite building materials, Energy and Buildings. 156 (2017) 293–305. https://doi.org/10.1016/j.enbuild.2017.09.097.
[16] B. Seng, C. Magniont, S. Lorente, Characterization of a precast hemp concrete. Part I: Physical and thermal properties, Journal of Building Engineering. 24 (2019) 100540. https://doi.org/10.1016/j.jobe.2018.07.016.
[17] C. Maalouf, C. Ingrao, F. Scrucca, T. Moussa, A. Bourdot, C. Tricase, A. Presciutti, F. Asdrubali, An energy and carbon footprint assessment upon the usage of hemp-lime concrete and recycled-PET façades for office facilities in France and Italy, Journal of Cleaner Production. 170 (2018) 1640–1653. https://doi.org/10.1016/j.jclepro.2016.10.111.
[18] R. Haik, G. Bar-Nes, A. Peled, I.A. Meir, Alternative unfired binders as lime replacement in hemp concrete, Construction and Building Materials. 241 (2020) 117981. https://doi.org/10.1016/j.conbuildmat.2019.117981.
[19] F. Delhomme, A. Hajimohammadi, A. Almeida, C. Jiang, D. Moreau, Y. Gan, X. Wang, A. Castel, Physical properties of Australian hurd used as aggregate for hemp concrete, Materials Today Communications. 24 (2020) 100986. https://doi.org/10.1016/j.mtcomm.2020.100986.
[20] F. Collet, S. Pretot, B. Mazhoud, L. Bessette, C. Lanos, R.A. Bergès, Comparing hemp composites made with mineral or organic binder on thermal, hygric and mechanical point of view, Academic Journal of Civil Engineering, 33(2015), 228-234.
[21] L. Arnaud, E. Gourlay, Experimental study of parameters influencing mechanical properties of hemp concretes, Construction and Building Materials. 28 (2012) 50–56. https://doi.org/10.1016/j.conbuildmat.2011.07.052.
[22] D. Taoukil, A. El bouardi, F. Sick, A. Mimet, H. Ezbakhe, T. Ajzoul, Moisture content influence on the thermal conductivity and diffusivity of wood–concrete composite, Construction and Building Materials. 48 (2013) 104–115. https://doi.org/10.1016/j.conbuildmat.2013.06.067.
[23] E. Gourlay, P. Glé, S. Marceau, C. Foy, S. Moscardelli, Effect of water content on the acoustical and thermal properties of hemp concretes, Construction and Building Materials. 139 (2017) 513–523. https://doi.org/10.1016/j.conbuildmat.2016.11.018.
[24] F. Collet, S. Pretot, Thermal conductivity of hemp concretes: Variation with formulation, density and water content, Construction and Building Materials. 65 (2014) 612–619. https://doi.org/10.1016/j.conbuildmat.2014.05.039.
[25] C. Véronique, Propriétés mécaniques, thermiques et acoustiques d'un matériau à base de particules végétales : approche expérimentale et modélisation théorique, (Ph.D. thesis), Institut National des Sciences Appliquées de Lyon, 2005.

[26] N.E. Hajj. Contribution à la conception et à l'élaboration d'une âme multicouche multifonctionnelle agrosourcée pour panneau sandwich : étude expérimentale et modélisation. PhD thesis, Université de Picardie Jules Verne, 2010.
[27] TH Pham. Modélisation multi-échelles des propriétés thermiques et élastiques de composites chaux-chanvre. PhD thesis, Université de Bretagne-Sud, 2014.
[28] A. Akkaoui, S. Caré, M. Vandamme, Experimental and micromechanical analysis of the elastic properties of wood-aggregate concrete, Construction and Building Materials. 134 (2017) 346–357. https://doi.org/10.1016/j.conbuildmat.2016.12.084.
[29] A.D. Tran-Le, S.-T. Nguyen, T. Langlet, A novel anisotropic analytical model for effective thermal conductivity tensor of dry lime-hemp concrete with preferred spatial distributions, Energy and Buildings. 182 (2019) 75–87. https://doi.org/10.1016/j.enbuild.2018.09.043.
[30] A. Couture, V. François, J.C. Cuillière, P. Pilvin, Modélisation de la microstructure de composites particulaires : Application à l'homogénéisation en conduction thermique, 13e colloque national en calcul des structures, 2017
[31] S. Mom, S Dartois, A. Ben Hamida, H. Dumontet, and H. Boussa. Modélisation itérative multi-échelles du béton de chanvre. In Congrès français de mécanique, 2011.
[32] T. Nguyen-Sy, A.D. Tran-Le, T. Nguyen-Thoi, T. Langlet, A multi-scale homogenization approach for the effective thermal conductivity of dry lime–hemp concrete, Journal of Building Performance Simulation. 11 (2018) 179–189. https://doi.org/10.1080/19401493.2017.1323009.
[33] Z.K. Low, N. Blal, N. Naouar, D. Baillis, Influence of boundary conditions on computation of the effective thermal conductivity of foams, International Journal of Heat and Mass Transfer. 155 (2020) 119781. https://doi.org/10.1016/j.ijheatmasstransfer.2020.119781.
[34] K. Miled, O. Limam, Effective thermal conductivity of foam concretes: Homogenization schemes vs experimental data and FEM simulations, Mechanics Research Communications. 76 (2016) 96–100. https://doi.org/10.1016/j.mechrescom.2016.07.004.
[35] B. Ismail, N. Belayachi, D. Hoxha, Optimizing performance of insulation materials based on wheat straw, lime and gypsum plaster composites using natural additives, Construction and Building Materials. 254 (2020) 118959. https://doi.org/10.1016/j.conbuildmat.2020.118959.
[36] S. Amziane, L. Arnaud, Les bétons de granulats d'origine végétale. Application aubéton de chanvre, Lavoisier, 2013.
[37] R. Hill, Elastic properties of reinforced solids: Some theoretical principles, Journal of the Mechanics and Physics of Solids. 11 (1963) 357–372. https://doi.org/10.1016/0022-5096(63)90036-X.
[38] Z. Hashin., Analysis of composite materials—a survey. Journal of applied mechanics, 50(3) :481–505, 1983..
[39] T. Kanit, S. Forest, I. Galliet, V. Mounoury, D. Jeulin, Determination of the size of the representative volume element for random composites: statistical and numerical approach, International Journal of Solids and Structures. 40 (2003) 3647–3679. https://doi.org/10.1016/S0020-7683(03)00143-4.
[40] I.M. Gitman, H. Askes, L.J. Sluys, Representative volume: Existence and size determination, Engineering Fracture Mechanics. 74 (2007) 2518–2534. https://doi.org/10.1016/j.engfracmech.2006.12.021.
[41] C. Pelissou, J. Baccou, Y. Monerie, F. Perales, Determination of the size of the representative volume element for random quasi-brittle composites, International Journal of Solids and Structures. 46 (2009) 2842–2855. https://doi.org/10.1016/j.ijsolstr.2009.03.015.

Journal Pre-proof

[42] M. Merzoud and MF. Habita. Elaboration de composite cimentaire à base de diss «ampelodesma mauritanica». Afrique Science : Revue Internationale Des Sciences Et Technologie, 4(2), 2008, (n.d.).
[43] A. Sellami, M. Merzoud, and S. Amziane. Improvement of mechanical properties of green concrete by treatment of the vegetals fibers. Construction and Building Materials, 47 :1117–1124, 2013., (n.d.).
[44] G. Delannoy, S. Marceau, P. Glé, E. Gourlay, M. Guéguen-Minerbe, D. Diafi, S. Amziane, F. Farcas, Impact of hemp shiv extractives on hydration of Portland cement, Construction and Building Materials. 244 (2020) 118300. https://doi.org/10.1016/j.conbuildmat.2020.118300.
[45] A. Akkaoui, Bétons de granulats de bois: étude expérimentale et théorique des propriétés thermo-hydro-mécaniques par des approches multi-échelles, Ph.D. thesis Université Paris-Est, 2014..
[46] B. Mazhoud, F. Collet, S. Pretot, C. Lanos, Mechanical properties of hemp-clay and hemp stabilized clay composites, Construction and Building Materials. 155 (2017) 1126–1137. https://doi.org/10.1016/j.conbuildmat.2017.08.121.

Journal Pre-proof

Journal Pre-proof

Modelling of thermal conductivity and nonlinear mechanical behavior of straw insulation composite by a numerical homogenization approach

Brahim ISMAIL[1], Naima BELAYACHI[1], Dashnor HOXHA[1], Laurent ARBARET[2]

[1] Université d'Orléans, INSA Centre Val de Loire, Université de Tours, Laboratoire de Mécanique Gabriel Lamé Polytech Orléans, 8 rue Léonard de Vinci, 45072 Orléans, France

[2] ISTO, UMR 7327, Université d'Orléans, CNRS, BRGM, 1A rue de la Férollerie, 45071, Orléans, France

Corresponding author :

Naima Belayachi

Tel : 330238492502

Fax : 330238417063

E-mail address : naima.belayachi@univ-orleans.fr

Postal address : Laboratoire LaMé, Polytech'Orléans

8 Rue Léonard De Vinci

45072, Orléans cedex 2, France

Journal Pre-proof

Tables

Composites	Binder	Straw/Binder (kg/kg)	Water/Binder (kg/kg)	Density (kg/m^3)
C1	Lime	0.2	1.1	450
C2	Lime+20%gelatin	0.4	1.1	300

Tab. 1. Composite designation and detailed mixture proportions

	C1	C2
Binder	33%	11%
Straw	30%	35%
Porosity (intergranular)	37%	54%

Tab. 2 . Volume fractions of the different phases for the two composites

	Thermal conductivitiy (λ/W/m.K)	
Composites	Vertical direction	Horizontal direction
C1	0.075±0.02	0.064±0.013
C2	0.057±0.017	0.051±0.019

Tab.3 . Thermal conductivity of composites in horizontal and vertical direction

	Matrix	Inclusion
Young's modulus E(MPa)	100	0.2
Poisson's ratio ν	0.3	0.1
Thermal conductivitiy (λ/W/m.K)	0.168	0.051

Tab. 4. Parameters used to determine effective properties.

Constituents	Thermal conductivity (W/m.K)
Matrix of C1-composite	0.168
Matrix of C2-composite	0.143
Straw	0.051
Air	0.026

Tab. 5. Thermal conductivities of constituents

Journal Pre-proof

	Straw	Air void
Young's modulus E (MPa)	0.2	10−6
Poisson's ratio ν	0.1	0.001

Tab.6 . Elastic parameters of the inclusions (Straw + air)

	Matrix_C1	Matrix_C2
Poisson's ratio ν	0.3	0.3
Young's modulus E(MPa)	100	85
Limite d'élasticité σ_Y (MPa)	0.25	0.09
Hardening modulus σ_∞ (MPa)	0.38	0.37
Hardening exponent m (MPa)	1400	1396
Linear hardening modulus k (MPa)	-5.5	-3.8

Tab. 7 Parameters used for the mechanical modelling

	Matrix_C1	Matrix_C2
Poisson's ratio ν	0.3	0.3
Young's modulus E(MPa)	30	35
Limite d'élasticité σ_Y (MPa)	0.15	0.145
Hardening modulus σ_∞ (MPa)	0.098	0.097
Hardening exponent m (MPa)	1800	1795
Linear hardening modulus k (MPa)	-2.9	-2.5

Tab. 8 Parameters used for the modeling of the mechanical behavior

Journal Pre-proof

Journal Pre-proof

Declaration of interests

☒ The authors declare that they have no known competing financial interests or personal relationships that could have appeared to influence the work reported in this paper.

☐The authors declare the following financial interests/personal relationships which may be considered as potential competing interests:

Journal Pre-proof